FLOOD WATER DEPTH ESTIMATION FOR THE HISTORICAL FLOOD IN QUANG BINH PROVINCE, VIETNAM IN 2020 USING SENTINEL-1A IMAGES

Nguyen Hung An*, Nguyen Tien Phat, Vu Duy Dong, Mai Quoc Khanh
Le Quy Don Technical University

ARTICLE INFO

Received: 20/6/2022
Revised: 03/8/2022
Published: 04/8/2022

KEYWORDS

SAR images
Multi-temporal images
Flood depth estimation
Water surface elevation
Spreading algorithm

ABSTRACT

Flood is a natural phenomena that usually causes serious consequences for human lives. The flood water depth estimation helps people to offer suitable solutions to deal with the damaging effects of the flood. The flood depth estimation methods using remote sensing images have been received a great interest and applied popularly for recent decades. The paper proposed a method to build the flood water depth map of Quang Binh province, Vietnam in the historical flood 2020 based on Sentinel-1A satellite images. This method is a combination of the classical Otsu method and the proposed spreading method. The former algorithm was first used to build the temporary water maps. Then, the latter algorithm was applied on these water maps to determine the flood inundation depths. This method of flood depth estimation proved computational simplicity and near-real-time speed, and provided relatively good accuracy.

ƯỚC LƯỢNG ĐỘ SÂU NGẬP LỤT Ở TỈNH QUẢNG BÌNH, VIỆT NAM TRONG TRẬN LŨ LỊCH SỬ NĂM 2020 SỬ DỤNG ẢNH SENTINEL-1A

Nguyễn Hùng An*, Nguyễn Tiến Phát, Vũ Duy Đông, Mai Quốc Khánh
Trường Đại học Kỹ thuật Lê Quý Đôn

THÔNG TIN BÀI BÁO

Ngày nhận bài: 20/6/2022
Ngày hoàn thiện: 03/8/2022
Ngày đăng: 04/8/2022

TỪ KHÓA

Ảnh SAR
Ảnh đa thời gian
Ước lượng độ sâu ngập lụt
Độ cao bề mặt nước
Thuật toán loang

TÓM TẮT

Lũ lụt là một hiện tượng tự nhiên thường gây ra các hậu quả nghiêm trọng cho cuộc sống của con người. Việc ước lượng độ sâu ngập lụt sẽ giúp cho con người đưa ra được các giải pháp phù hợp để xử lý các ảnh hưởng tàn phá của lũ lụt. Các phương pháp ước lượng độ sâu ngập lụt sử dụng ảnh viễn thám đã nhận được nhiều sự quan tâm và được sử dụng phổ biến trong các thập kỷ gần đây. Bài báo này đề xuất một phương pháp để xây dựng bản đồ độ sâu ngập lụt của tỉnh Quảng Bình, Việt Nam trong trận lũ lịch sử năm 2020 dựa trên ảnh Sentinel-1A. Phương pháp trong bài báo là sự kết hợp của phương pháp Otsu kinh điển và phương pháp loang được đề xuất mới. Phương pháp Otsu trước tiên được sử dụng để xây dựng các bản đồ nước hiện thời. Sau đó, phương pháp loang được thực hiện trên các bản đồ nước hiện thời này để xác định độ sâu ngập lụt. Phương pháp ước lượng độ sâu ngập lụt được đề xuất trong bài báo này đã chứng minh được sự đơn giản về tính toán, tốc độ gần thời gian thực và cung cấp độ chính xác tương đối tốt.

DOI: https://doi.org/10.34238/tnu-jst.6196

* Corresponding author. *Email: hungan@lqdtu.edu.vn*

1. Introduction

Nowadays, global warming increases the occurrence frequency of floods and their level of destruction [1] – [3]. In order to evaluate severity of floods, the two parameters of most interest could be coverage and flood water depth, among which the second parameter estimation could be the most challenging. Methods of flood depth estimation can be divided into two basic groups as with contact water level gauges and non-contact water level gauges [4]. The former group uses hardware systems such as sensors, level indicators and other measurement stations, which make contact with water, or are kept underwater or on the water surface, to measure the water levels. For the latter group, the instrumentations do not directly contact with water such as ultrasonic water level gauges and radar water level gauges. In comparison with former one, the latter one is more suitable for flood depth estimation for big-scale areas.

As one of the most popularly used methods of non-contact water level measurement, remote sensing image processing methods use the multi-temporal images of flooded areas to estimate the flood depths. Their advantages are not expensive, efficient, and easy to automatically deploy in practice for the large scale areas. Two type of images popularly used for non-contact flood inundation depth estimation method are optical and Synthetic Aperture Radar (SAR) images. In contrast to optical images, SAR images are nearly unaffected by the weather conditions, and even night and daytime. Therefore, the flood depth estimation using SAR images has been popular for recent decades. Due to the very low radar return reflection, flooded areas in SAR images occur with dark appearances. This is an important signature to detect the flood inundation in SAR images [5] – [7].

Generally, estimation of the flood depth is usually implemented through two main steps: (i) detecting flooded areas and (ii) computing flood depths. The threshold based and change detection based techniques could be two of the most widely used ones to detect flooded areas. The threshold based techniques compare a threshold, computed from one image, with the intensity values of pixels to classify water pixels. Although their advantage is simple and automatic threshold computation, accuracy of threshold estimation depends on environmental factors or the specific satellite acquisition geometry [8] – [11]. Change detection based techniques use multi-temporal images captured in the same flooded place at the different times, including before, during and after the flood time, and detect the differences between them by the backscattering values reduced. However, the accuracy of these methods can be impacted by land-cover changes with different backscattering values at two captured times [8], [12] – [14]. The threshold based approach was applied in this paper because of its simplicity and easy implementation in reality.

After the flood inundation area detection, the flood inundation depth at a pixel is computed by subtracting the water surface elevation to the corresponding value of Digital Elevation Models (DEMs) at that pixel. Therefore, accuracy of flood depth estimation depends on accuracy of detecting flood water areas and calculating the water surface elevation, and the accuracy of the DEM used as well.

The paper proposed a novel method of flood depth estimation for the area of Quang Binh province in Vietnam during the historic flood in October 2020. This method is a combination of the Otsu algorithm [15], which used the threshold to classify water points, and the spreading algorithm proposed for estimating flood inundation depths. The objectives of the study are to detect flooded areas and improve accuracy of flood depth estimation.

The remaining of this paper is organized as follows. In Section 2, the study case and datasets used are described. The methodology and applied algorithms are presented in Section 3. The experimental results and performance evaluation of the proposed algorithm are presented in Section 4. Section 5 draws conclusions from our results, and outlines main research directions in the near future.

2. Methodology

2.1. The study case

Quang Binh is a coastal province in the North Central part of Vietnam with the total area of 8000 km^2 and the population of 882,505 people. In the worst flooding for 41 years taking place from 16 to 20 October 2020, it damaged seriously lives of people, properties and infrastructures. For instance, there were total 106,000 houses seriously affected, 25 found dead people. The flood peak was recorded on Kien Giang river, which is a tributary of Nhat Le river, at 4.89 m for several consecutive days. This peak eclipsed the historical record peak in 1979 by up to 0.98 m.

This paper estimated flood depths in the areas of Quang Binh province during the flood from 12 to 24 October 2020.

2.2. Datasets

Datasets used for this paper were the set of Sentinel-1A satellite images and ALOS PALSAR DEM of Quang Binh province, Vietnam. In addition, the paper also used the test data collected manually and the reference measurement station data.

2.2.1. Sentinel-1A images

Sentinel-1A images with ID "COPERNICUS/ S1 - GRD" in the dataset of Google Earth Engine are dual-polarized (VV and VH) SAR ones with space resolution of 10 m per each pixel, as shown in Figure 1.

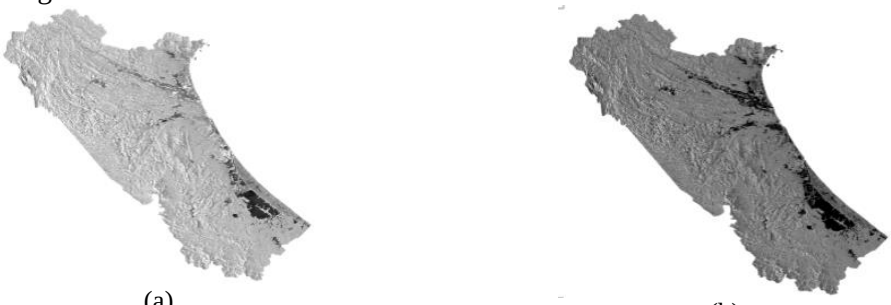

(a) (b)

Figure 1. *Sentinel-1A images captured of Quang Binh province on 18 October 2020 with (a) VV and (b) VH channels*

The set of Sentinel-1A images consists of 66 images, in which 62 VV images were captured from 01/09/2019 to 31/08/2020 and used to build the permanent water map, two VH images captured in 18/10/2020 and two VH images captured in 24/10/2020 were used to build the temporary flood water maps. Because each image only cover a half of Quang Binh area, so each pair of images were processed particularly and then combined together to produce a complete image of Quang Binh.

2.2.2. ALOS PALSAR Digtal Elevation Model

The ALOS PALSAR DEM was downloaded from Distributed Active Archive Centers AFS, at website https://vertex.daac.asf.alaska.edu. The DEM provides the terrain height at the each pixel with the resolution of 12.5 m.

2.2.3. Test data

Test data consists of water and dry points were taken from the permanent water map and temporay water map, as shown in Figure 2. These points were manually collected with QGIS and Google Earth Pro Tools and satellite images. It is noticed that test points being permanent water points were chosen in the centre of ponds, lakes and rivers, while test points being temporary

water points on the flood day were chosen near the side of flooded areas and did not coincide permanent water ones.

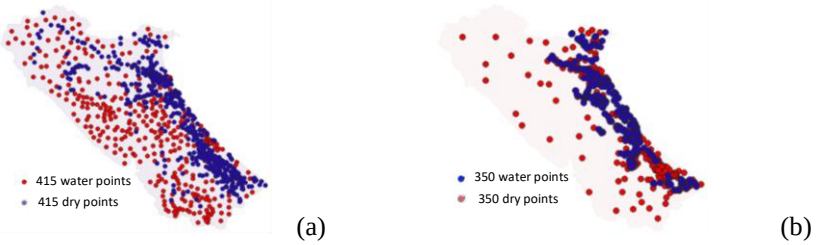

Figure 2. *Test points in (a) the temporary water area map, and (b) permanent water area map*

2.2.4. Reference data

Estimated flood depths were verified based on flood depth data measured by six river water level measurement stations on 12/10/2020 (the day the rain started), 18/10/2020 (flood peak) and 24/10/2020 (the water decreased) as shown in Table 1. The data in this table was provided by Irrigation Sub-Department of Quang Binh.

Table 1. *Reference flood depth data measured at six measurement stations on three days: 12/10/2020 (the rain starting day), 18/10/2020 (the peak flood day) and 24/10/2020 (the drawing flood day)*

Station name	Latitude	Longtitude	Flood depth 12/10/2020 (m)	Flood depth 18/10/2020 (m)	Flood depth 24/10/2020 (m)
Dong Hoi	$17^0$28’	$106^0$37’	0	1.14	0.63
Kien Giang	$17^0$07’	$106^0$45’	0	2.50	0.76
Le Thuy	$17^0$13’	$106^0$47’	0	2.40	1.99
Dong Tam	$17^0$54’	$106^0$01’	0	0.94	0
Mai Hoa	$17^0$48’	$106^0$11’	0	2.14	0.40
Tan My	$17^0$42’	$106^0$28’	0	0.59	0

2.3. Methodology

In order to estimate flood inundation depths, it is necessary to classify water points from dry points (or ground points). The flood depths were computed by subtracting the estimated water level heights of the water areas to the corresponding DEM values. The diagram of building the flood depth classification map was proposed as described in Figure 3.

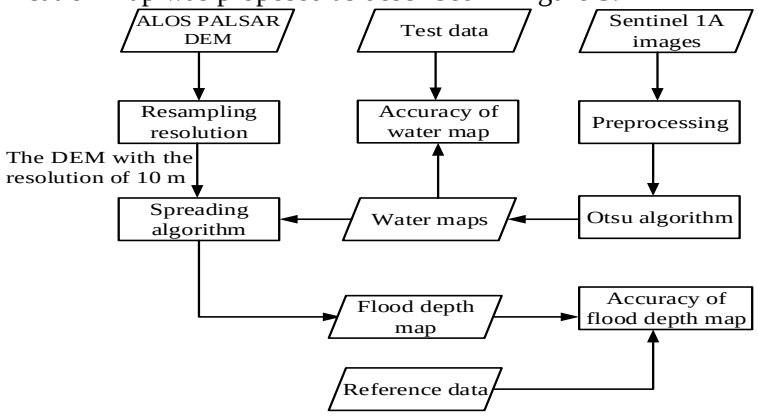

Figure 3. *Block diagram of building the flood depth classification map*

The proposed procedure of building the flood depth map consists of four steps as following:

- *Step* 1: Match the resolutions of ALOS PALSAR DEM and Sentinel-1A images;
- *Step* 2: Pre-process Sentinel-1A images;

- *Step* 3: Apply the Otsu method to the pre-processed Sentinel-1A images to build the set of temporary water maps and the permanent water map;
- *Step* 4: Apply the spreading algorithm to the water maps to build flood depth maps.

2.3.1. Preprocessing

The pre-processing process includes common image processing steps such as geo-referencing, suppressing edge and thermal noises. In addition, extraction of reflection values, VV and VH for each image, and use of filters by slope to reduce effects of mountain shades were implemented.

2.3.2. Otsu algorithm

The Otsu algorithm [15] determined a threshold to separate water pixels and non-water pixels. The Otsu algorithm was briefly described as follows.

Let us consider an image $f(x,y)$ with L different gray levels from 0 to L-1. Select a threshold $T_h = t$ ($0 \le t \le L$-1) to divide the image into two classes C_1 and C_2. C_1 is the set of pixels whose intensity values are less than or equal to t. C_2 is the set of remaining pixels. The occurrence probabilities of these two classes are respectively described in Equation (1).

$$P_{C_1}(t) = \sum_{i=0}^{t} P_i$$
$$P_{C_2}(t) = \sum_{i=t+1}^{L-1} P_i = 1 - P_{C_1}(t) \quad (1)$$

where $P_i = n_i/N$. n_i is the number of occurrence of the pixel with the intensity of i. N is the total number of pixels in the image.

The mean levels of the class of C_1 and C_2 are respectively defined as follows.

$$m_1(t) = \sum_{i=0}^{t} i \times P_i / P_{C_1}(t)$$
$$m_2(t) = \sum_{i=t+1}^{L-1} i \times P_i / P_{C_2}(t) \quad (2)$$

The threshold T_h is defined as the value that the the between-class variance of C_1 and C_2 achieves the maximum value:

$$\sigma_B^2(T_h) = \max_{0 \le t \le L-1} \left(\sigma_B^2(t) \right) \quad (3)$$

where:
$$\sigma_B^2(t) = P_{C_1}(t) P_{C_2}(t) \left(m_1(t) - m_2(t) \right)^2 \quad (4)$$

If there are many $\sigma_B^2(t)$ equal together, t maximal is chosen as the threshold T_h.

The pixels of the water classification map have the values of 0 (non-water pixels) if corresponding pixels of VV/VH images larger than or equal to the T_h, and have the values of 1 (water pixels) in the otherwise case.

2.3.3. Spreading algorithm

The spreading algorithm was implemented on the previous water maps with the assumption of the height of the current water pixel as the same as that of the eight adjacent water pixels.

Let assume the pixel with the coordinates of x and y, $I(x,y)$, to be a considered water pixel. Initially, all water pixels were marked as 0. The spreading algorithm was implemented through three steps:

- *Step* 1: $I(x,y)$ is marked as 1. If there exists one of its eight adjacent pixels to be dry at least, collect and store this dry pixel. If there is no its adjacent water pixels marked as 0, then move to *Step* 3;

- *Step* 2: For each adjacent water pixel with the mark value of 0 found in *Step* 1, replace $I(x,y)$ with it, and loop *Step* 1;
- *Step* 3: The heights of all stored dry points (boundary points) are then averaged to provide the water surface height.

After that, the pixel flood depth was computed as difference of the computed water surface height and its DEM value. Removing permanent water pixels from the water depth map produces the final flood depth map. It is noticed that the permanent water map was built from the set of 62 images. Each pixel in the permanent water map has the value of 1 (water points) when there are more than a half of corresponding pixels classified as water in these images; otherwise it is brought the value of 0 (non-water points).

2.3.4. Performance evaluation

The proposed method was evaluated in terms of the accuracy of building the water map by the Otsu algorithm and the accuracy of estimated flood depths.

The accuracy of the Otsu algorithm in building the water maps was estimated by four parameters of *Overall Accuracy* (*OA*), *Recall*, *Precision* and F_1 score:

$$OA = \frac{T_p + T_n}{T_p + T_n + F_p + F_n} \tag{5}$$

$$Recall = \frac{T_p}{T_p + F_n} \tag{6}$$

$$Precision = \frac{T_p}{T_p + F_p} \tag{7}$$

$$F_1 = 2 \times \frac{Precision.Recall}{Precision + Recall} \tag{8}$$

where T_p is the number of correctly classified water pixels, T_n is the number of correctly classified non-water pixels. F_p is the number of wrong classified non-water pixels, F_n is the number of wrong classified water pixels.

For evaluating the accuracy of estimated flood depths, they were compared with reference data collected from the six measurement stations in Table 1.

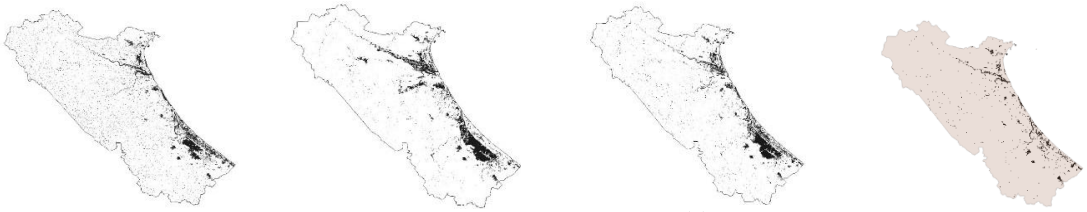

(a) (b) (c) (d)

Figure 4. *The water maps on (a) 12/10/2020 (the rain starting day), (b) 18/10/2020 (the peak flood day), (c) 24/10/2020 (drawing flood day), and (d) the permanent water map. Pixels with black color are water ones*

3. Experimental results and performance evaluation

3.1. Accuracy of water maps built by the Otsu method

For each image, a threshold was computed by the Otsu method, then applied to classify water pixels for the whole image. The image pixel with VH scattering value lower than Otsu's threshold was classified as water one. For example, with three thresholds of -18.85, -20.91 and -20.87 dB computed from three corresponding images captured on 12/10/2020, 18/10/2020 and 24/10/2020, the corresponding water maps were produced as shown in Figure 4(a), (b) and (c), respectively.

In addition, the permanent water map built from the 62 images, as presented at the end of Section 2.3.3, was shown in Figure 4(d). In these figures, pixels with black color are water ones.

Table 2. *Water area classification accuracy of the Otsu algorithm based on test data*

	Water map on 18/10/2020	Permanent water map
Precision	83.33%	70.1%
Recall	98.5%	98.8%
F_1	0.90	0.82
OA	89.8%	78.4%

The accuracy of water point classification results based on the Otsu method was evaluated by the test data. The evaluated results of the flood water map on 18/10/2020 and permanent water map were presented in Table 2 with the parameters of *Precision*, *Recall*, F_1 score and *OA*, which were all quite good. Generally, these parameters estimated for the map built on 18/10/2020 are higher than for the permanent map, except for *Recalls* approximately equal. This can be explained that on 18/10/2020 - peak floor day, the area of water occupies 21% of researched area, it made the Otsu method give the approximately optimal layering threshold. However, for the dry season, the water area is too small in comparison with the total area, so it results in considerably decreased accuracy of water classification by the Otsu method.

3.2. Accuracy of flood depth estimation

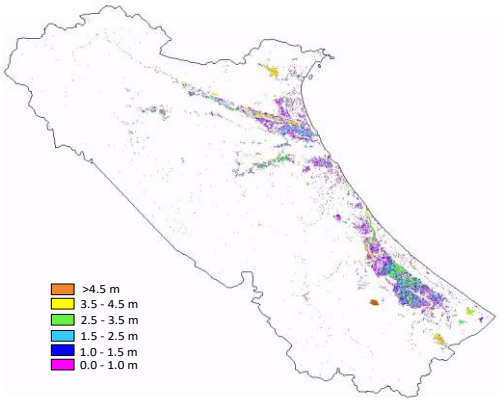

Figure 5. *The flood depth map built for the day of 18 October 2020 with 1000 subregions*

In order to improve the accuracy of flood depth estimation, the water maps were divided into subregions on which the spreading algorithm was applied to estimate the flood depths for these subregions. The different sizes of subregions were investigated to find out the optimal size so that the accuracy of flood depth estimation was the highest. Here, the image was divided into subregions by rows. For instance, the investigated image with the size of 12000 × 16000 pixels was divided into sub-images with the size of N × 16000 pixels, where N is from 1 to 200. If N = 1 the whole image is divided into 12000 subregions with the size of 1 × 16000 pixels, while for N = 200, the image is divided into 60 subregions with the size of 200 × 16000 pixels.

By investigating different values of N, its optimal value was found as N = 12. This is equivalent to the image divided into 1000 subregions with the size of 12 × 16000 pixels. The flood depth map on 18/10/2020 was shown in Figure 5. This map was built based on applying the spreading algorithm on the subregions with the size of 12 × 16000 pixels.

To evaluate the accuracy of the flood depth estimation results by the proposed method, the flood depths estimated at the positions next to six measurement stations at Dong Hoi, Kien Giang, Le Thuy, Dong Tam, Mai Hoa and Tan My were compared with the corresponding flood

depth values measured by these six stations shown in Table 1, which were assumed as reference (or truth) data values. The estimation error was defined as difference between the estimated results and corresponding truth data values.

Figure 6 showed flood depth estimation results at the positions next to the six measurement stations according to different numbers of subregions in comparison with the reference data (or truth data). As can be seen from Figure 6 that the estimated flood depths at the six stations in the case of the image divided into 1000 sub-regions were the closest to the reference data.

Table 3. *Root mean square errors (RMSEs) versus the different numbers of subregions*

No of sub-regions	0	200	400	600	800	1000	1200
RMSE	1.9340	1.5641	2.0119	2.5286	1.3530	0.5366	2.4955

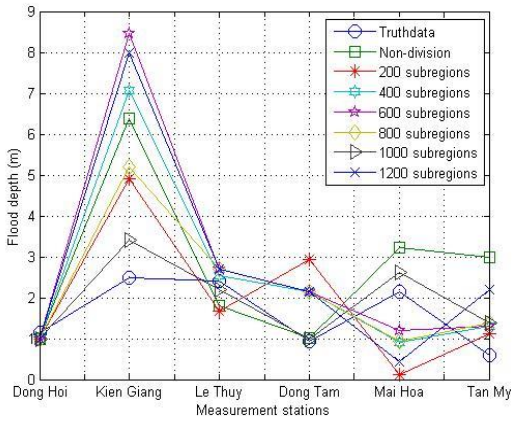

Figure 6. *The results of flood depth estimation at the positions of six measurement stations according to different numbers of subregions*

In order to quantitatively compare flood depth estimation results for different cases of image subdivision, the root mean square errors (RMSEs) were used, which were computed based on the reference data in Table 1, and were shown in Table 3. This table showed that the image subdivision with 1000 sub-regions results in the smallest value of RMSE (0.5366), while with the number of sub-regions less or larger than 1000, the corresponding RMSEs are larger than this value. Because Quang Binh's terrain is mainly mountainous and slope from West to East, the larger the sub-region is, the larger the error of water surface elevation estimated as the average height of pixels on the boundary of water regions is, so the larger the error of the flood depth estimation is. It can be seen from Table 3, when the number of sub-regions is small (less than 1000), it means their area is large, the RMSEs are large. Also, because of the complex terrain, for the small sub-region, the water surface elevation estimation can receive large errors if there are abnormal height changes of adjacent pixels on the boundary. As Table 3 showed, when the number of sub-regions is larger than 1000, it means their area is small, the RMSEs are large.

In summary, the flood water depth estimation by spreading algorithm was performed on the temporary flood water maps with permanent water points removed. Applying the spreading algorithm on the sub-regions with optimal sizes could increase the accuracy of the estimation.

4. Conclusion

The paper proposed a novel solution to estimating flood depths based on Otsu and spreading algorithms. The advantages of this solution are computational simplicity and near real-time speed. Experiment results of the proposed solution were evaluated by comparing them with the reference data obtained from measurement stations and proved relatively good accuracy.

The proposed method of flood depth estimation can be effectively applied in relatively flat areas. However, there are also mistakes of distinguishing water with some objects such as wet

mud and sand. In addition, this method results in low flood depth estimation accuracy when applied for more complicated areas such as big cities. These are issues necessary to be studied and solved in the near future.

REFERENCES

[1] L. Alfieri, P. Burek, L. Feyen, and G. Forzieri, "Global warming increases the frequency of river floods in Europe," *Hydrology and Earth System Sciences,* vol. 19, pp. 2247-2260, 2015.

[2] P. Allamano, P. Claps, and F. Laio, "Global warming increases flood risk in mountainous areas," *Geophysical Research Letters,* vol. 36, pp. 1 - 5, 2009.

[3] Z. W. Kundzewicz, Y. Hirabayashi, and S. Kanae, "River floods in the changing climate—observations and projections," *Water Resources Management,* vol. 24, pp. 2633-2646, 2010.

[4] B. B. Nair and S. Rao, "Flood water depth estimation—A survey," *2016 IEEE International Conference on Computational Intelligence and Computing Research (ICCIC)*, IEEE, 2016, pp. 1-4.

[5] P. Matgen, R. Hostache, G. Schumann, L. Pfister, L. Hoffmann, and H. Savenije, "Towards an automated SAR-based flood monitoring system: Lessons learned from two case studies," *Physics and Chemistry of the Earth, Parts A/B/C,* vol. 36, pp. 241-252, 2011.

[6] V. Herrera-Cruz, F. Koudogbo, and V. Herrera, "TerraSAR-X rapid mapping for flood events," *Proceedings of the international society for photogrammetry and remote sensing (earth imaging for geospatial information),* Hannover, Germany, 2009, pp. 170-175.

[7] D. C. Mason, R. Speck, B. Devereux, G. J.-P. Schumann, J. C. Neal, and P. D. Bates, "Flood detection in urban areas using TerraSAR-X," *IEEE Transactions on Geoscience and Remote Sensing,* vol. 48, pp. 882-894, 2009.

[8] L. Giustarini, H. Vernieuwe, J. Verwaeren, M. Chini, R. Hostache, P. Matgen, N. E. Verhoest, and B. De Baets, "Accounting for image uncertainty in SAR-based flood mapping," *International Journal of Applied Earth Observation and Geoinformation,* vol. 34, pp. 70-77, 2015.

[9] J.-B. Henry, P. Chastanet, K. Fellah, and Y.-L. Desnos, "Envisat multi-polarized ASAR data for flood mapping," *International Journal of Remote Sensing,* vol. 27, pp. 1921-1929, 2006.

[10] S. Martinis, A. Twele, and S. Voigt, "Towards operational near real-time flood detection using a split-based automatic thresholding procedure on high resolution TerraSAR-X data," *Natural Hazards and Earth System Sciences,* vol. 9, pp. 303-314, 2009.

[11] N. Pierdicca, L. Pulvirenti, M. Chini, L. Guerriero, and L. Candela, "Observing floods from space: Experience gained from COSMO-SkyMed observations," *Acta Astronautica,* vol. 84, pp. 122-133, 2013.

[12] L. Giustarini, R. Hostache, P. Matgen, G. J.-P. Schumann, P. D. Bates, and D. C. Mason, "A change detection approach to flood mapping in urban areas using TerraSAR-X," *IEEE transactions on Geoscience and Remote Sensing,* vol. 51, pp. 2417-2430, 2012.

[13] P. Matgen, G. Schumann, J.-B. Henry, L. Hoffmann, and L. Pfister, "Integration of SAR-derived river inundation areas, high-precision topographic data and a river flow model toward near real-time flood management," *International Journal of Applied Earth Observation and Geoinformation,* vol. 9, pp. 247-263, 2007.

[14] S. Long, T. E. Fatoyinbo, and F. Policelli, "Flood extent mapping for Namibia using change detection and thresholding with SAR," *Environmental Research Letters,* vol. 9, 2014, Art. no. 035002.

[15] N. Otsu, "A threshold selection method from gray-level histograms," *IEEE transactions on systems, man, and cybernetics,* vol. 9, pp. 62-66, 1979.